AGU PUBLICATIONS

JGR

Journal of Geophysical Research: Atmospheres

RESEARCH ARTICLE
10.1002/2014JD022888

Key Points:
- Sea salt, cloud, and radiative properties vary with the ENSO cycle
- Decadal sea salt variability is dominated by Pacific Ocean variability
- Sea salt may affect ENSO-related cloud variability in the tropical Pacific

Correspondence to:
L. M. Russell,
lmrussell@ucsd.edu

Citation:
Xu, L., D. W. Pierce, L. M. Russell, A. J. Miller, R. C. J. Somerville, C. H. Twohy, S. J. Ghan, B. Singh, J.-H. Yoon, and P. J. Rasch (2015), Interannual to decadal climate variability of sea salt aerosols in the coupled climate model CESM1.0, *J. Geophys. Res. Atmos.*, *120*, 1502–1519, doi:10.1002/2014JD022888.

Received 24 NOV 2014
Accepted 15 JAN 2015
Accepted article online 23 JAN 2015
Published online 21 FEB 2015

Interannual to decadal climate variability of sea salt aerosols in the coupled climate model CESM1.0

Li Xu[1], David W. Pierce[1], Lynn M. Russell[1], Arthur J. Miller[1], Richard C. J. Somerville[1], Cynthia H. Twohy[1,2], Steven J. Ghan[3], Balwinder Singh[3], Jin-Ho Yoon[3], and Philip J. Rasch[3]

[1]Scripps Institution of Oceanography, University of California, San Diego, La Jolla, California, USA, [2]Northwest Research Associates, Redmond, Washington, USA, [3]Atmospheric Science and Global Change Division, Pacific Northwest National Laboratory, Richland, Washington, USA

Abstract This study examines multiyear climate variability associated with sea salt aerosols and their contribution to the variability of shortwave cloud forcing (SWCF) using a 150 year simulation for preindustrial conditions of the Community Earth System Model version 1.0. The results suggest that changes in sea salt and related cloud and radiative properties on interannual timescales are dominated by the El Niño–Southern Oscillation cycle. Sea salt variability on longer (interdecadal) timescales is associated with low-frequency variability in the Pacific Ocean similar to the Interdecadal Pacific Oscillation but does not show a statistically significant spectral peak. A multivariate regression suggests that sea salt aerosol variability may contribute to SWCF variability in the tropical Pacific, explaining up to 20–30% of the variance in that region. Elsewhere, there is only a small sea salt aerosol influence on SWCF through modifying cloud droplet number and liquid water path that contributes to the change of cloud effective radius and cloud optical depth (and hence cloud albedo), producing a multiyear aerosol-cloud-wind interaction.

1. Introduction

Aerosols have a strong effect on the Earth's radiation balance. This happens both directly through reflecting incoming solar radiation back to space and indirectly through altering cloud microphysical properties by acting as cloud condensation nuclei (CCN) or ice nuclei and changing cloud albedo [*Twomey*, 1974] and lifetime [*Albrecht*, 1989]. Overall, these aerosol effects contribute a net negative climate forcing [*Penner et al.*, 2001] and offset warming of the Earth climate system. The magnitude of the aerosol indirect effect is recognized as one of the largest uncertainties in our understanding of changing climate.

The Intergovernmental Panel on Climate Change (IPCC) Fifth Assessment Report [*Boucher et al.*, 2013] presents a best estimate of effective radiative forcing from both aerosol-radiation interactions and aerosol-cloud interactions of $-0.9\,\mathrm{W\,m^{-2}}$ with a 5% to 95% uncertainty range of -1.9 to $-0.1\,\mathrm{W\,m^{-2}}$, in which a 90% uncertainty range of -1.2 to $0\,\mathrm{W\,m^{-2}}$ is ascribed to aerosol-cloud interactions alone. This wide uncertainty range arises from difficulties representing the nonlinear microphysical processes that aerosols or aerosol precursor gases undergo to determine CCN concentration through emission, nucleation, condensation, and coagulation and from poorly characterized spatial and temporal variation and uncertainties in aerosol concentrations. It is also a result of differences between satellite- and model-estimated aerosol effects on clouds. These arise at least partly from estimating characteristics of preindustrial clouds from those of present-day clouds [*Penner et al.*, 2011]. The low estimated sensitivity of present-day clouds to aerosols relies on observations that are not representative of the preindustrial atmosphere except at remote marine environments [*Penner et al.*, 2012]. *Ghan et al.* [2013] and *Carslaw et al.* [2013] confirmed this finding; moreover, the Carslaw sensitivity analysis suggested that the majority (45%) of uncertainty in aerosol indirect forcing since 1750 arises from uncertainties in emissions of natural aerosols, including sea salt, volcanic sulfur dioxide, marine dimethylsulfide, biogenic volative organic carbon, and biomass burning, while only 34% arises from uncertainty in anthropogenic emissions. Quantification of aerosol indirect forcing and its variability requires an understanding of effects not only due to the substantial anthropogenic perturbations but also due to natural aerosols in the pristine preindustrial conditions. This highlights the importance of understanding aerosols with natural origins in the preindustrial era.

Two regionally based observational studies have found that interannual variability in aerosols can be associated with El Niño–Southern Oscillation (ENSO) [*Li et al.*, 2011; *Wu et al.*, 2013]. The positive ENSO

phase (El Niño) is characterized by warm sea surface temperature anomalies over the eastern Pacific and dry conditions over Indonesia. This leads to extensive biomass burning over the Indonesian regions [*Chandra et al.*, 1998, 2009; *Logan et al.*, 2008; *van der Werf et al.*, 2006] and over the northern part of South America [*Le Page et al.*, 2008], an enhancement of Barbados dust concentrations [*Prospero and Lamb*, 2003] and Australian dust emissions [*Mitchell et al.*, 2010], as well as significant increase of sea salt emissions [*Penner et al.*, 2001].

A number of studies provide evidence that aerosol variability may influence multiyear variations of regional climate. *Booth et al.* [2012] used a global climate model to show that aerosols covary with the modeled multidecadal variability of North Atlantic sea surface temperatures over the period of 1860–2005 and suggested that aerosols may be a primary driver of twentieth century North Atlantic climate variability, although *Zhang et al.* [2013] challenged this point of view. *Wilcox et al.* [2013] performed an analysis of CMIP5 (the fifth Coupled Model Intercomparison Project) [*Taylor et al.,* 2012] global climate model simulations and found that models including both the aerosol direct and indirect effects better reproduce interdecadal variability in historical global mean near surface temperatures and precipitation than those with the aerosol direct effect only. They also demonstrated that the diversity in aerosol burden and representation of aerosol-cloud interaction among models is associated with a substantial variation in simulations of multidecadal variability. These findings, together with the *Ghan et al.* [2013] and *Carslaw et al.* [2013] results on the importance of variability in natural aerosols, suggest that an in-depth examination of interannual to decadal variability in natural aerosols in a state-of-the-art global climate model is warranted.

Sea salt constitutes the largest fraction of Earth's natural aerosols by mass in the atmosphere since 71% of the Earth's surface is covered by oceans [*O'Dowd et al.*, 1997]. Moreover, sea salt is an important source of CCN in remote marine areas [*Clarke et al.*, 2006]. Despite its importance, there is significant uncertainty in the sea salt emission flux, with estimates ranging over orders of magnitude [*Lewis and Schwartz*, 2004; *Textor et al.*, 2006; *Grythe et al.*, 2013]. The estimated global sea salt burden also spans a wide range from 4.1 to 11.6 Tg [*Textor et al.*, 2006]. These ranges are a result of uncertainties in the wind speed dependence of source fluxes, different emission parameterizations, and the different treatments of aerosol removal processes used in global models. *Penner et al.* [2001] found that sea salt emission may increase with increasing wind speed in a warmer climate, although this result was model dependent. *Jones et al.* [2007] examined the modeled change of sea salt aerosol in response to a doubling of CO_2 and found an increase in sea salt burdens at high latitudes (poleward 60°N and 60°S), which was driven by stronger winds resulting from the reduction in regional sea ice. Given that sea salt particles comprise a large fraction of CCN number in remote ocean areas, variations in sea salt burden in the atmosphere with wind speed or temperature are likely to alter cloud radiative forcing and cause a negative climate forcing through changes in cloud droplet number [*Korhonen et al.*, 2010]. In other words, the increased sea salt aerosol particles resulting from an increase in oceanic wind speed or sea surface temperature (possible results of atmospheric warming) [*Young et al.*, 2011] subsequently enhance the emission of cloud condensation nuclei and hence increase cloud droplet number concentration and possibly in-cloud liquid water path. The changes overall may eventually lead to smaller cloud effective radius and larger cloud albedo or longer cloud lifetime, thereby producing a net cooling effect. This sea salt-cloud-radiation-climate interaction constitutes a negative climate feedback [*Latham and Smith*, 1990; *Korhonen et al.*, 2010].

The objective of this study is to investigate the multiyear (interannual to interdecadal) variability of sea salt aerosols in the Earth's climate and to illustrate how this variability impacts clouds and radiative forcing. Given the importance of understanding the preindustrial variability as noted above, in this work we use a 150 year simulation of preindustrial conditions (year 1850 emissions) produced by the Community Earth System Model version 1.0 (CESM1) [*Hurrell et al.*, 2013]. Exploring these issues in a coupled climate model framework allows us to perform a global analysis over a time period long enough to address interdecadal variability, something that is not possible from observations, especially since the present atmosphere already has a significant anthropogenic aerosol burden. *Flato et al*. [2013, their Figure 9.7] show that CESM1 (when coupled to the Community Atmospheric Model version 5 (CAM5) atmospheric model, as used here) performs better than the average CMIP5 model in simulating 11 of 13 key measures of global climate when compared to observations over the historical period (1850–2005). A drawback to this approach is that the results are subject to being viewed through the lens of a particular model's set of parameterizations, making comparisons to observations important in interpreting the results.

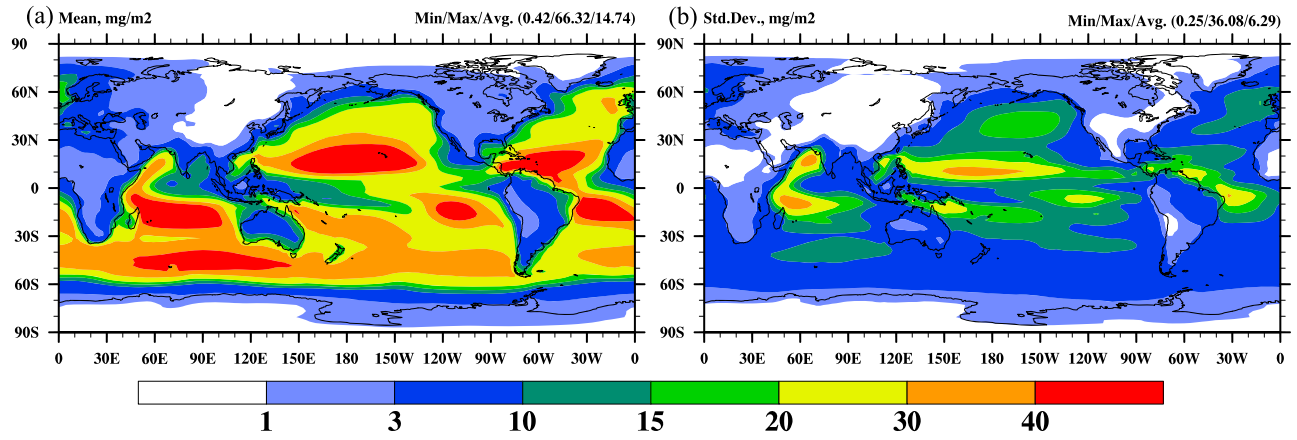

Figure 1. (a) Climatological mean and (b) standard deviation of column-integrated sea salt burden (mg/m^2). The global minimum, maximum, and mean values are given at the upper right corner of each panel.

The rest of this paper is organized as follows. The CESM1 model is briefly described in section 2, with a focus on aspects of the model relevant to the aerosol experiments performed here. Analysis of the sea salt variability at different timescales is given in section 3. The discussion and conclusions are addressed in section 4.

2. The Community Earth System Model

The 150 year simulation for preindustrial conditions was performed using the Community Earth System Model version 1.0 (CESM1), which is composed of atmosphere, ocean, land surface, and sea ice components [*Hurrell et al.*, 2013]. The coupled model produces natural internal climate variability such as the El Niño–Southern Oscillation (ENSO), North Atlantic Oscillation, and the Pacific Decadal Oscillation (PDO), but emissions for most aerosol components (primary organic carbon and black carbon) and precursor gases (dimethyl sulfide (DMS), SO_2, and volatile organic compound (VOC)) are prescribed at estimated values from 1850. The atmosphere model resolution is 1.9° latitude by 2.5° longitude in the horizontal, with 30 vertical layers ranging from the surface to 3.6 hPa. The model uses the modal aerosol module (MAM3) with three modes (size classes), including Aitken (dry diameter size range of 0.015–0.053 μm), accumulation (0.058–0.27 μm), and coarse modes (0.80–3.65 μm). Within each mode, the mass mixing ratios of internally mixed aerosol species and the total number mixing ratio are treated prognostically. The total number of transported tracers is 15 in MAM3, including the transported gas species (i.e., SO_2, H_2O_2, DMS, and H_2SO_4) and an aggregate semivolatile organic species. The surface emission of sea salt particles with a diameter < 2.8 μm are parameterized as found in the laboratory studies of *Martensson et al.* [2003], in which the total particle flux is a nonlinear function of 10 m wind speed and sea surface water temperature. For diameters > 2.8 μm, the sea salt emission follows the parameterization by *Monahan et al.* [1986] in which the total particle flux depends on 10 m wind speed alone. In other words, warm temperatures tend to decrease ultrafine sea salt aerosol and increase coarse particle emission preferentially, while high winds enhance the salt emission across an entire size range [*Martensson et al.*, 2003]. A more detailed description of the model's aerosol representation can be found in *Liu et al.* [2012]. The model treats stratiform clouds using the detailed microphysics schemes described by *Morrison and Gettelman* [2008]. The treatment of deep and shallow convective cloud parameterizations is described in *Zhang and McFarlane* [1995] and *Park and Bretherton* [2009], respectively. Both deep and shallow convective parameterizations use different very simple bulk (single moment) microphysics treatments that convert condensate to precipitation as a function of the local convective mass flux and temperature. More detailed cloud processes in CAM5 appear in *Park et al.* [2014]. The variables used for the analysis in this work are saved as monthly averages.

3. Results

3.1. Sea Salt Burden and Emission

Figure 1 shows the 150 year climatological mean and standard deviation of annually averaged, column-integrated sea salt burden. Relatively large values are located over the storm track regions where wind speed and therefore emission are higher (e.g., Southern Ocean) and within dry subtropical regions between 30°S and 30°N

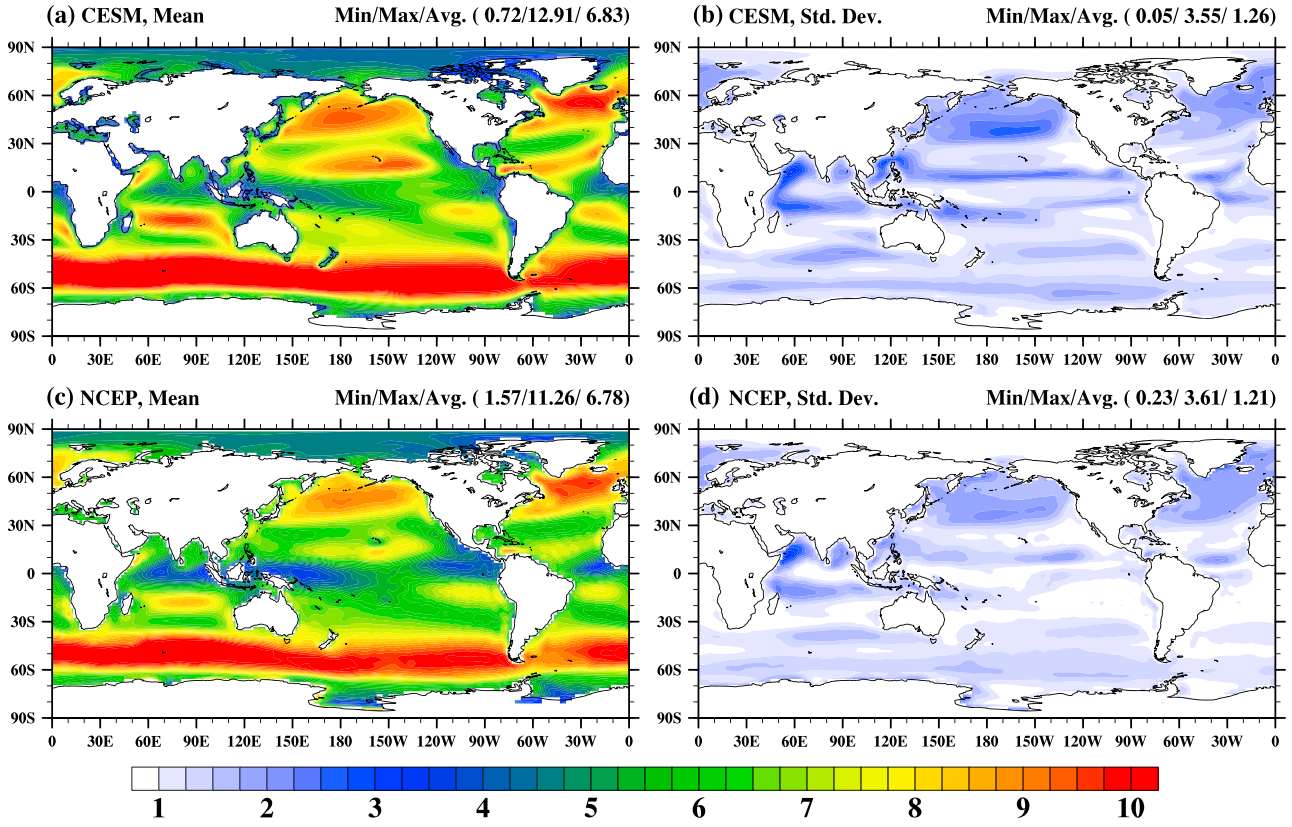

Figure 2. The climatological mean and standard deviation of 10 m wind speed (a and b) from the CESM model and (c and d) from the NCEP reanalysis. The minimum, maximum, and mean values averaged over all ocean points are given at the upper right corner of each panel.

where wet scavenging is lower and the sea surface temperature (SST)-dependent emission is higher [*Spada et al.*, 2013; *Struthers et al.*, 2013]. The column-integrated sea salt burden ranges from 0.42 to 66.32 mg m^{-2} with a mean of 14.74 mg m^{-2}. Higher values of the standard deviation tend to be colocated with the highest mean sea salt burden, especially over the subtropical regions, where the standard variation of precipitation is greater (not shown here). It is worth noting that variability is low in the Southern Ocean (30°S–60°S), although the sea salt burden is high. This is probably because the year-to-year emission and removal processes of sea salt aerosols share similar variability there, reducing the variations in sea salt burden over this region. The total annual mean sea salt burden is estimated as 9.69 Tg, in reasonable accord with the 10.37 Tg reported in *Liu et al.* [2012] and in the upper part of the 4.1 to 11.6 Tg range estimated by *Textor et al.* [2006].

In CESM1 sea salt emission is proportional to $U_{10}^{3.41}$, where U_{10} is the 10 m wind speed. Increased variability of wind speed about the mean may lead to the higher variability of sea salt emissions. The model's climatological mean and standard deviation of 10 m wind speed is compared to the National Center for Environmental Prediction (NCEP) reanalysis (1948–2014) in Figure 2. Although ideally this would be evaluated with high-frequency winds, we are limited to a monthly comparison due to data availability. Community Earth System Model (CESM) generally overestimates the mean and standard deviation (particularly in the Southern Hemisphere storm track) but reproduces the general spatial pattern of the NCEP winds throughout much of the ocean, such as higher means in the tropical Pacific and Atlantic and tropical Indian and Southern Oceans. Note that probably because the winds in the CESM simulation are for the preindustrial era while those from NCEP are based on the years 1948–2014; the different time frames of the calculation could result in some bias of the mean and variance.

3.2. Interannual Variability of Sea Salt Aerosols

In order to investigate the interannual variability of sea salt aerosol and their related cloud and radiative properties, we used an empirical orthogonal function (EOF) analysis of the monthly anomalies of the relevant variables. EOF analysis of anomaly data is an effective tool to reveal characteristics of spatial and temporal variability by decomposing the simulated variables into a set of orthogonal spatial and temporal patterns.

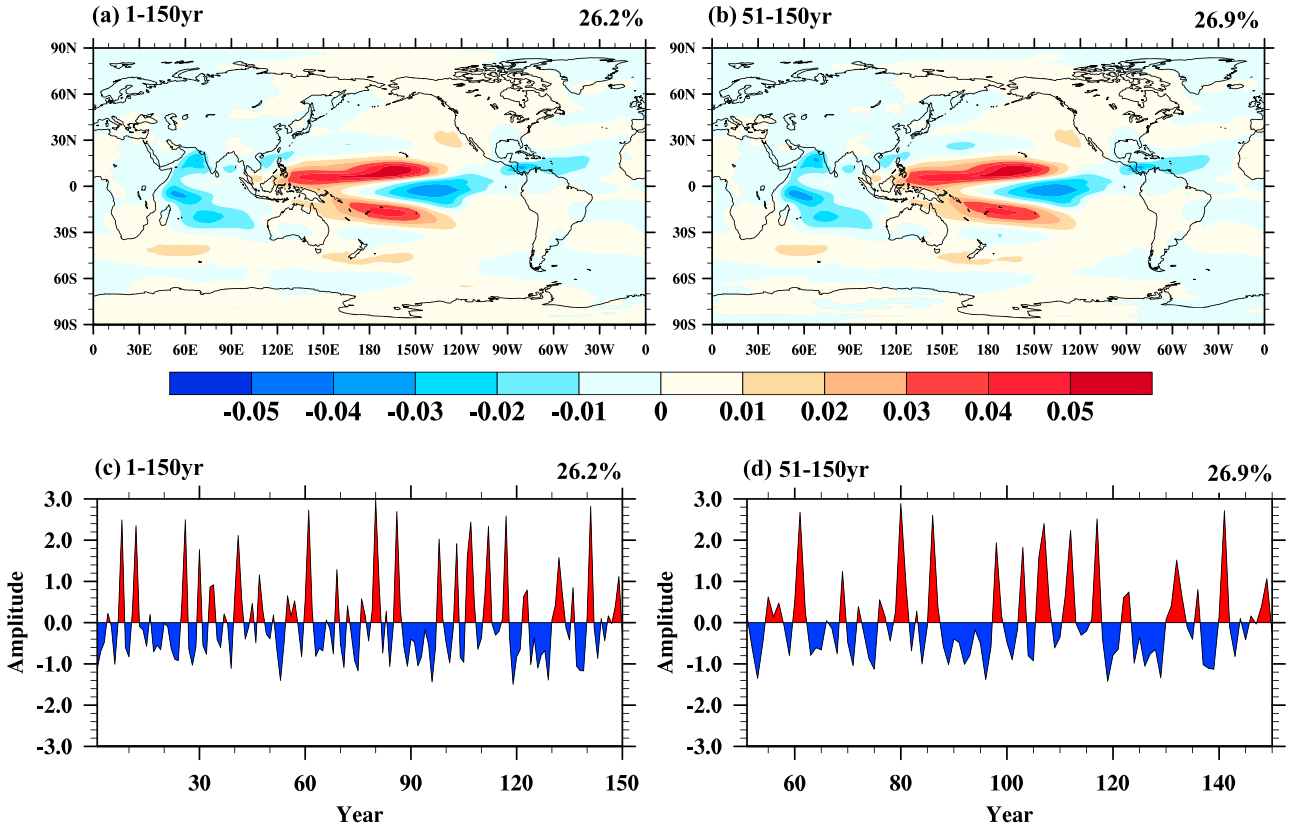

Figure 3. (a, b) The leading EOF mode of yearly sea salt burden anomalies and (c, d) the time series of corresponding principal component (PC) for the 150 year simulation and the last 100 year simulation (i.e., from the 51st year to the 150th year), respectively. The variance explained by the leading mode EOF is given at the upper right corner of each panel.

We generally present here only the leading EOF mode, which represents the highest variance of investigated variables and is not distorted by the orthogonality constraints imposed on subsequent modes. A drawback of EOF analysis is that only the product of the spatial pattern and temporal time series is constrained by observations, resulting in a sign ambiguity between the spatial pattern and time series; the same results are obtained if both are flipped in sign. To avoid this ambiguity, in cases where results from multiple variables are presented simultaneously, simple correlations were examined to select the signs displayed in the figures herein, making the phasing between different variables consistent.

Figure 3 shows the leading EOF of yearly sea salt burden anomalies and its corresponding principal component (PC) for the 150 year simulation. The leading EOF mode explains 26% of the annual variance of sea salt burden. The dominant pattern is located within the latitude band (30°S–30°N), where the western Pacific Ocean shows a scissor-like positive pattern and the eastern Pacific Ocean exhibits a negative counterpart, indicating that opposing variations in sea salt burden occurred in these two ocean regions. It is worth noting that the dominant EOF mode has little expression outside the tropics, even though the highest sea salt burden is in the midlatitudes of the Southern Ocean. There is little variability evident in the Atlantic Ocean. The first 50 years of the 150 year simulation show a trend in global sea salt burden, which is removed in Figures 3b and 3d showing only the last 100 years of the run. The differences from the full run are negligible, and subsequent figures omit this comparison. The leading EOF modes of 10 m wind speed, cloud droplet number, and shortwave cloud radiative forcing shown in Figure 4 have similar major spatial variability in the Pacific Ocean as that of sea salt burden, suggesting an interannual aerosol-cloud-wind interaction.

Overall, the results of the sea salt burden EOF analysis showing a bipolar feature in the tropical Pacific hint that there may be a relationship between sea salt aerosol burden (and related cloud and radiative properties) and the El Niño–Southern Oscillation (ENSO), since ENSO is the dominant mode of interannual variability in the tropical Pacific climate system. Moreover, the spatial pattern of the leading mode EOF of

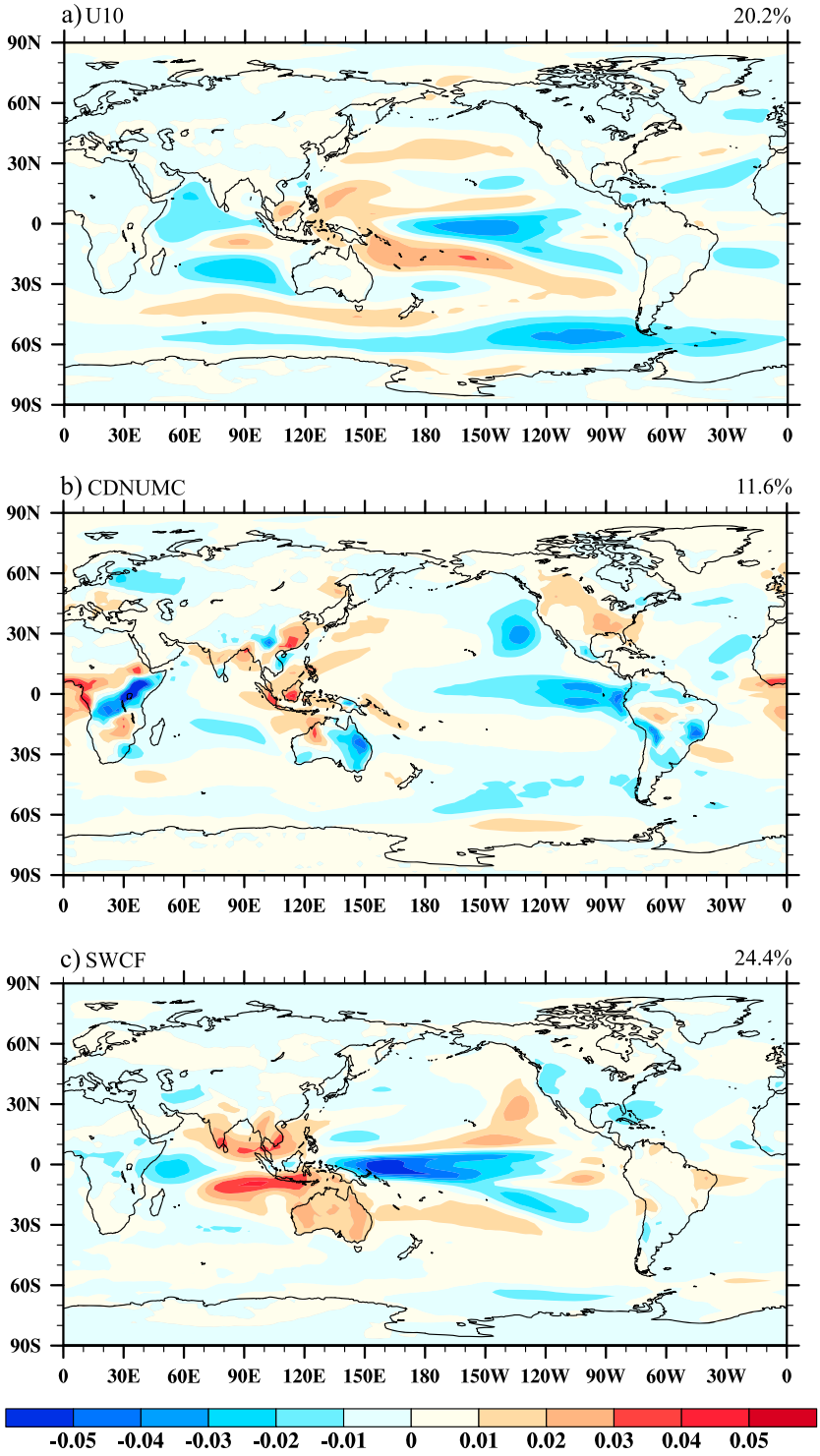

Figure 4. The leading mode of EOF analysis of yearly 10 m wind speed (U10), column-integrated cloud droplet number (CDNUMC), and shortwave cloud forcing (SWCF). The variance explained by the leading mode EOF is given at the upper right corner of each panel.

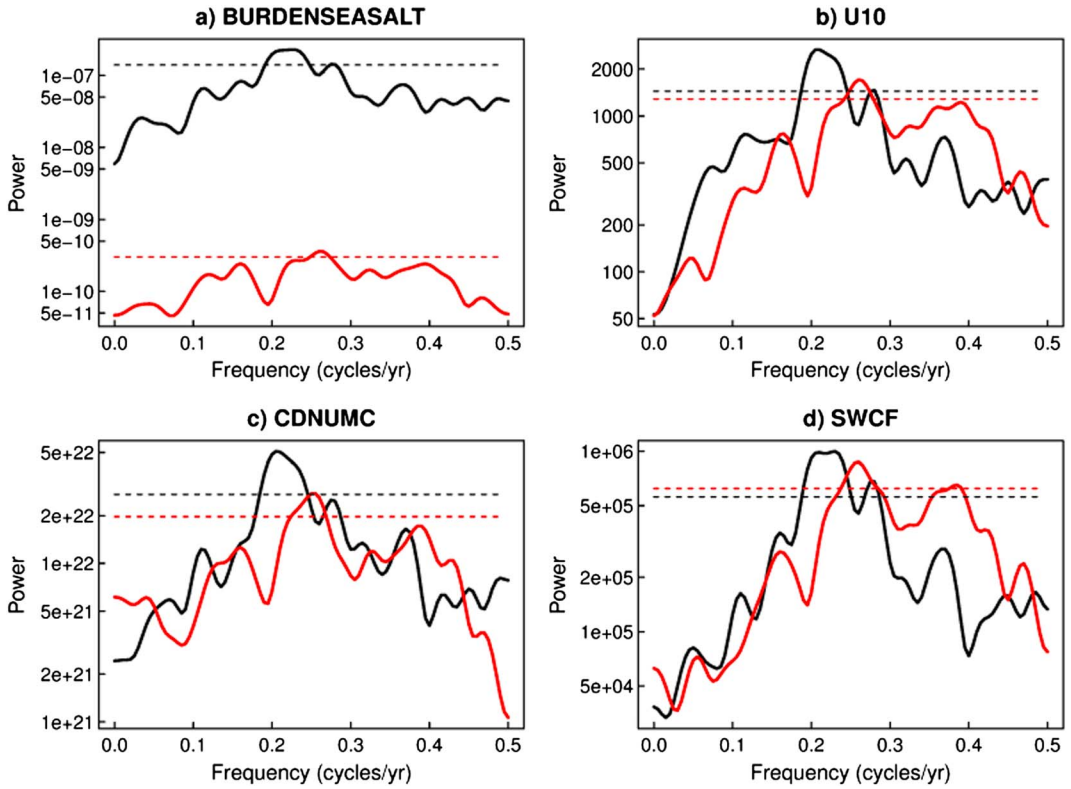

Figure 5. The power spectrum of the leading principal component (PC) of leading mode empirical orthogonal function (EOF) of (a) sea salt burden, (b) 10 m wind speed, (c) column-integrated cloud droplet number, and (d) shortwave cloud forcing. The black lines represent the spectra using yearly data from the 150 year fully interactive run. Red lines show results from a 150 year run when sea salt aerosol concentrations were specified. The corresponding black and red dashed lines indicate the 95% significance levels.

sea salt burden resembles the effects of ENSO on precipitation, which has a similar location and shape, including a weak response in the western Indian Ocean that is opposite in sign to the response over Indonesia [e.g., *Shen et al.*, 2014].

Figure 5 (black lines) shows the power spectra of the principal components associated with the leading EOFs of yearly sea salt burden, 10 m wind speed, column-integrated cloud droplet number, and shortwave cloud radiative forcing anomalies. All variables show a consistent peak around the frequency of 0.22 cycles per year (~4.5 years per cycle), which agrees well with the model's simulated ENSO period of 3–6 years [*Deser et al.*, 2012]. This suggests that ENSO is the main identifiable process affecting the interannual variability of these variables. In addition to this 150 year simulation in which sea salt emissions were predicted based on 10 m wind speed and sea surface temperature, we also conducted a 150 year simulation with prescribed monthly mean sea salt aerosol mass mixing ratios obtained from the simulation with interactive sea salt. A similar spectral analysis of this run is shown as the red lines in Figure 5. The variability in sea salt burden is naturally much reduced in this case, by about 3 orders of magnitude. The spectra of U10, cloud droplet number, and SWCF are somewhat weaker than in the fully interactive run and tend to have more power at higher frequencies. This suggests that the relationship between SWCF and ENSO may be partially influenced by the ENSO control of sea salt mixing ratios. However, because of large variability in ENSO, even over 150 year timescales, additional targeted simulations would be useful to verify this finding.

The association between sea salt aerosols and ENSO could arise through changes in the deposition of sea salt (primarily through precipitation in the tropics), surface emission of sea salt (primarily mediated through wind speed), or both. Sea surface temperature changes associated with ENSO also affect sea salt emissions in the model. Using the sea salt emission parameterization described in section 2, the estimated total sea salt number emission changes by about 40% due to wind speed fluctuations associated with ENSO but only about 5% due to sea surface temperature fluctuations. This indicates that typical ENSO-related wind changes

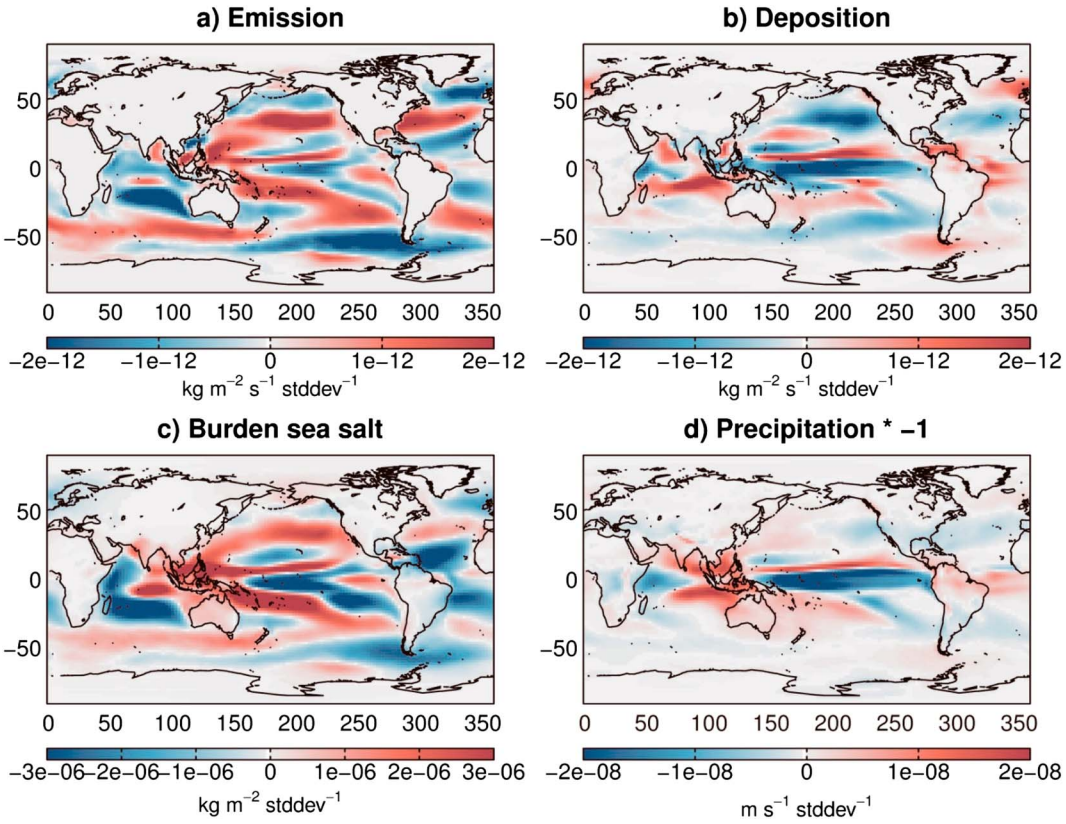

Figure 6. Regression coefficient between the model's ENSO index and (a) surface emission of sea salt aerosols, (b) deposition of sea salt aerosols, (c) total column burden of sea salt aerosols, and (d) precipitation rate (multiplied by −1, so it can be more directly compared to the deposition rate).

have a larger effect on sea salt emissions than typical ENSO-related sea surface temperature changes. Although sea surface temperature has a relatively smaller influence on the production of sea salt aerosol than wind speed [*Martensson et al.*, 2003], it plays an important role in reproducing observed sea salt surface concentration, especially in the tropic regions [*Spada et al.*, 2013; *Struthers et al.,* 2013]. Figure 6 shows the regression coefficient between the model's monthly ENSO index (i.e., the principal component associated with the leading EOF of sea surface temperature anomalies), monthly anomalies of surface emission and wet deposition of sea salt aerosols, and the total column sea salt aerosol burden. Since results for the three aerosol modes differ little, only results for mode 1 are shown.

The variability in total column burden is most similar to the variability in emissions (Figure 6c versus Figure 6a), which suggests that changes in surface emissions of sea salt are the main driver of the association between ENSO and sea salt aerosols. However, some effects due to changes in deposition rates with ENSO can be seen as well, for example, in the stronger negative response along the equatorial Pacific found in total burden compared to that seen in the emissions, and in the positive relationship between total burden and ENSO in the eastern Indian ocean along the equator, both of which are features found in the deposition pattern (Figure 6b). The relationship between ENSO and precipitation anomalies is shown in Figure 6d, where values have been multiplied by −1, so the pattern can be more easily compared to the deposition pattern (Figure 6b). The comparison shows that ENSO-related changes in the sea salt aerosol deposition rate are dominated in the tropics by changes in precipitation.

Figure 7 shows the correlation coefficient between the principal component of yearly SST anomalies and anomalies of (a) sea salt burden, (b) 10 m wind speed, (c) column-integrated cloud droplet number, and (d) shortwave cloud radiative forcing. The correlations display hemispherically symmetric patterns with appreciable values in extratropical regions, reminiscent of the Interdecadal Pacific Oscillation (IPO) [*Power et al.*, 1999]. The IPO pattern in sea surface temperature is "ENSO-like" but with more equal loading between

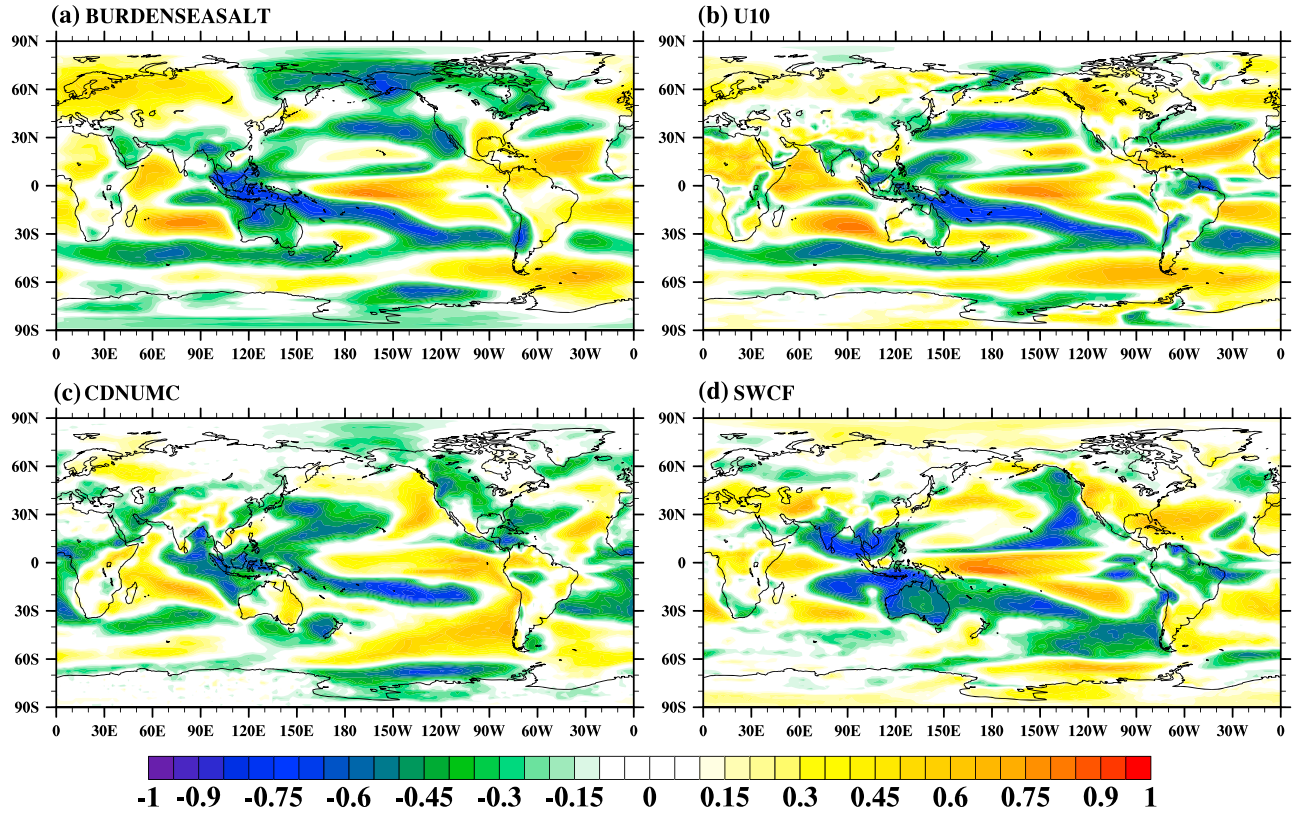

Figure 7. The correlation coefficient between the first mode yearly EOF PC of SST and anomaly of (a) sea salt burden, (b) 10 m wind speed, (c) column-integrated cloud droplet number, and (d) shortwave cloud radiative forcing.

the tropics and extratropics and becomes more evident when examining interdecadal variability rather than the interannual variability most closely associated with ENSO [*Zhang et al.,* 1997; *Folland et al.*, 2002; *Parker et al.*, 2007]. This further demonstrates that sea salt, cloud, and radiative properties exhibit variability related to Pacific Ocean climate fluctuations on interannual to decadal timescales.

Although observations of global aerosol optical depths are limited, it is worthwhile to compare the available data to the model results. Figure 8 shows the composite of average (December-January-February (DJF)) aerosol

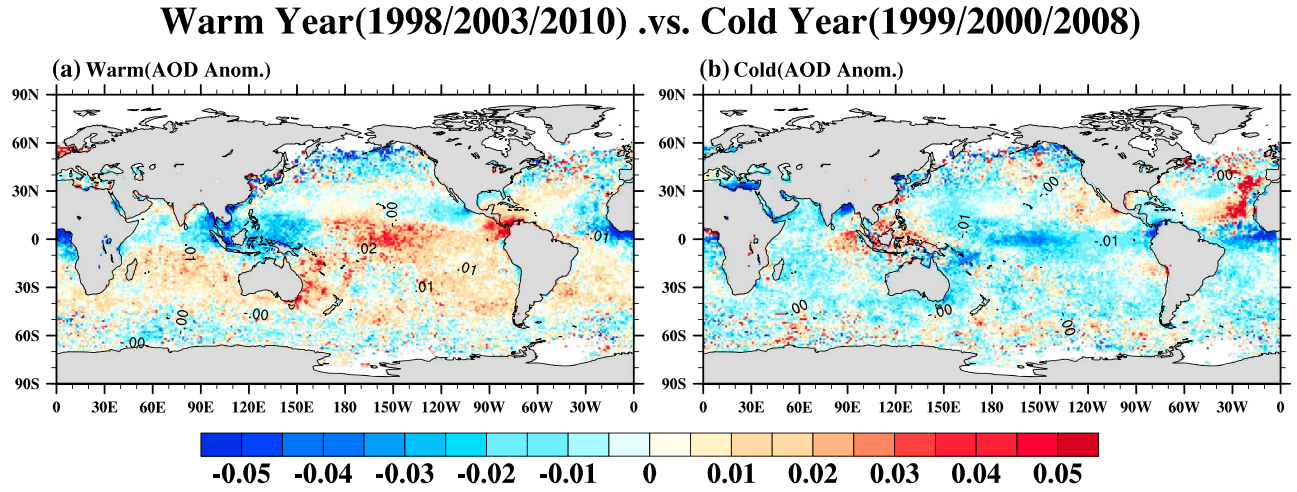

Figure 8. Composite of average aerosol optical depth anomaly from SeaWiFs satellite data for (a) warm years and (b) cold years in winter (DJF), respectively.

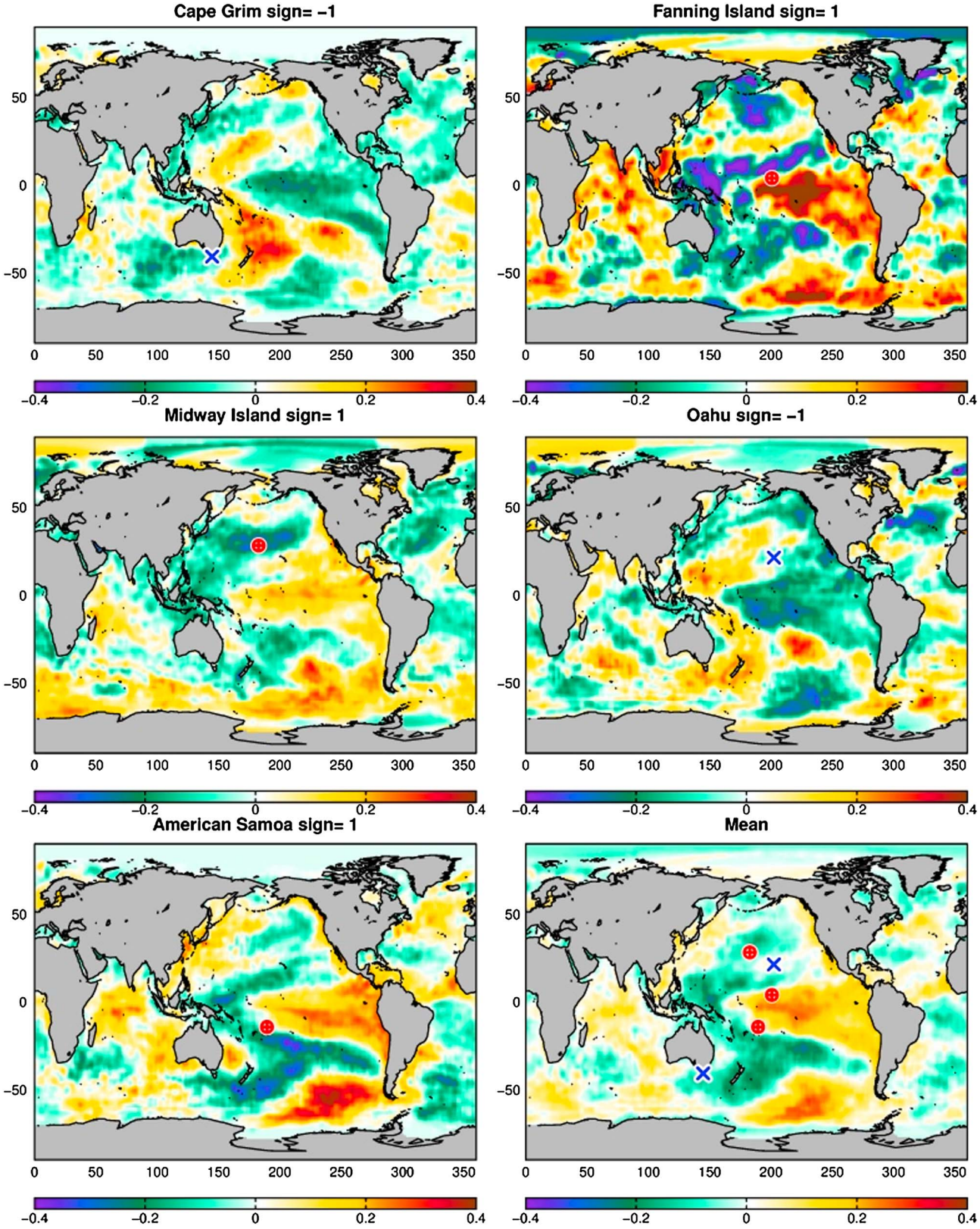

Figure 9. The correlation between the in situ monthly sea salt mass concentration anomalies measured at five stations (as indicated in the panel titles) and observed monthly sea surface temperature anomalies, and their mean response (sixth panel). Cape Grim and Oahu are marked as blue cross while Fanning Island, Midway Island, American Samoa are marked as a red circle.

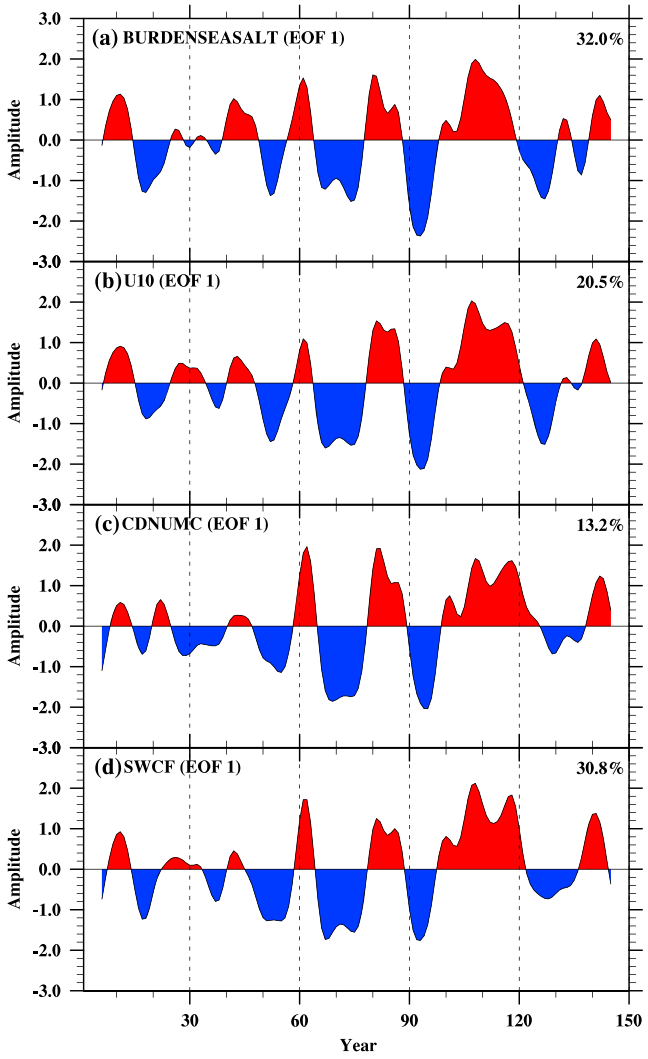

Figure 10. The time series of the first mode yearly EOF PC through the 150 year simulation of (a) burden sea salt, (b) 10 m wind speed, (c) column-integrated cloud droplet number, and (d) shortwave cloud radiative forcing with 10 year low-pass filter. The value explained by the leading mode EOF is given at the upper right corner of each panel.

optical depth (AOD) anomaly from the Sea-viewing Wide Field-of-view Sensor (SeaWiFS) satellite data for (a) warm El Nino years (i.e., 1998, 2003, and 2010) and (b) cold La Nina years (i.e., 1999, 2000, and 2008). In this study, we used the Level 3 1°×1° spatial resolution monthly mean SeaWiFS AOD data set at 550 nm from September 1997 to August 2010, which is a product of the Making Earth System Data Records for Use in Research Environments (MEaSUREs) project available at http://disc.sci.gsfc.nasa.gov/measures. The satellite-observed composites of AOD anomalies during DJF between warm years and cold years clearly show distinct and opposite patterns over the tropic eastern Pacific Ocean where the ENSO is expected as a dominant mode in the tropical atmosphere. Available observations therefore support the conclusion that the aerosol optical depth over oceans (dominated by sea salt aerosols, with the exception of the major dust and near-industrial regions) has a close link with ENSO. We note, however, that in the region of Indonesia, the satellite-observed AOD may also include seasonal influences from agricultural burning [*Marlier et al.*, 2013], a mechanism not included in the model simulations.

Li et al. [2011] found a strong correlation between aerosol Ångström exponent anomaly (which is controlled by changes in particle composition that result from changing mixtures of particle sources and are typically accompanied by changes in particle size distributions) and ENSO over the tropical Pacific in satellite measurements. No significant ENSO correlation with AOD (which is sensitive to total aerosol loading) was identified over that region. *Hsu et al.* [2012] found a high correlation between SeaWiFS AOD anomaly and the Multivariate ENSO Index in the tropics near Indonesia and off the coast of Central America. This is in accordance with our findings in the aforementioned composite analysis.

The satellite observations include all aerosol types and so are not completely consistent with our analysis of sea salt alone. We therefore also investigate the interannual variability observed with in situ point measurements of sea salt mass concentration produced during the early 1980s to the late 1990s by the Global Aerosol Climatology Project (http://gacp.giss.nasa.gov/data_sets/Joseph_Prospero.html). The five stations located in the Pacific Basin (Cape Grim, 1983–1996; Fanning Island, 1981–1986; Midway Island, 1981–2000; Oahu, 1981–1995; and American Samoa, 1983–1999) with good data quality as recommended in *Spada et al.* [2013] were used for the analysis. The original daily data are binned into monthly averages, and then the temporal anomalies are computed. The first five panels of Figure 9 show the correlation between the sea salt mass concentration anomalies measured at the station indicated in the title and global observed sea surface temperature anomalies. Each station shows a hemispherically symmetric

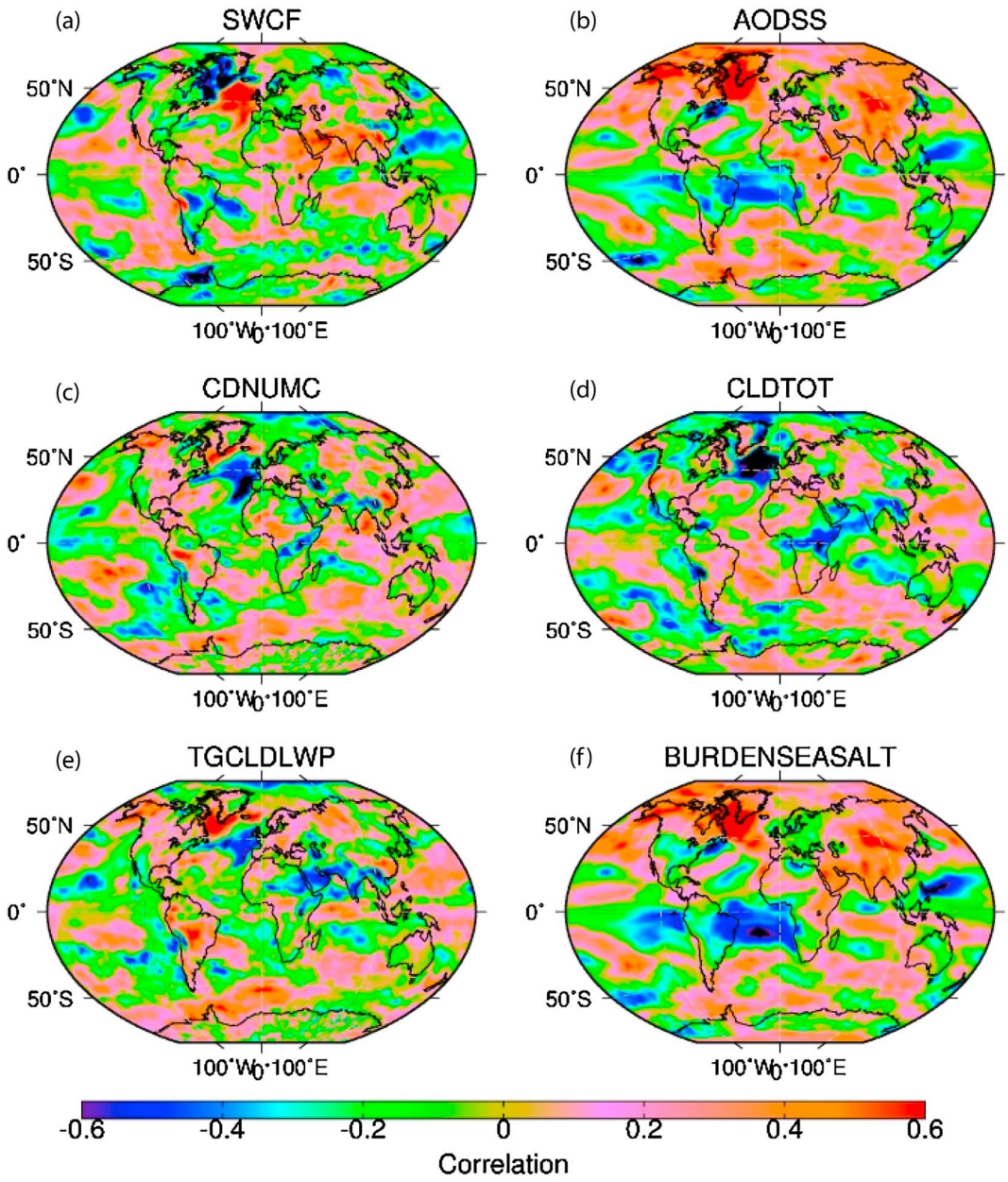

Figure 11. The correlation coefficient between the model's AMO index and (a) shortwave cloud radiative forcing, (b) sea salt aerosol optical depth, (c) column-integrated cloud droplet number, (d) total cloud fraction, (e) cloud liquid water path, and (f) sea salt burden.

relationship between the sea salt mass concentration and sea surface temperature that is similar in spatial pattern to the IPO, although they have different signs because some stations are located in a place that has a positive relationship between sea salt aerosols and tropical Pacific SST, and other stations in a place with a negative relationship (the sign is indicated in the panel title, and stations with a positive relationship are plotted as a red circle, while a blue cross indicates a negative relationship). By taking the appropriate sign into account we can average the correlations of all the stations to reduce noise and purely local effects and get an overall relationship between observed sea salt aerosols and sea surface temperature anomalies (Figure 9, sixth panel). The resulting IPO-like pattern demonstrates that the observed variability of sea salt aerosols specifically, and not just total AOD, is associated with interannual to interdecadal climate fluctuations in the Pacific Ocean.

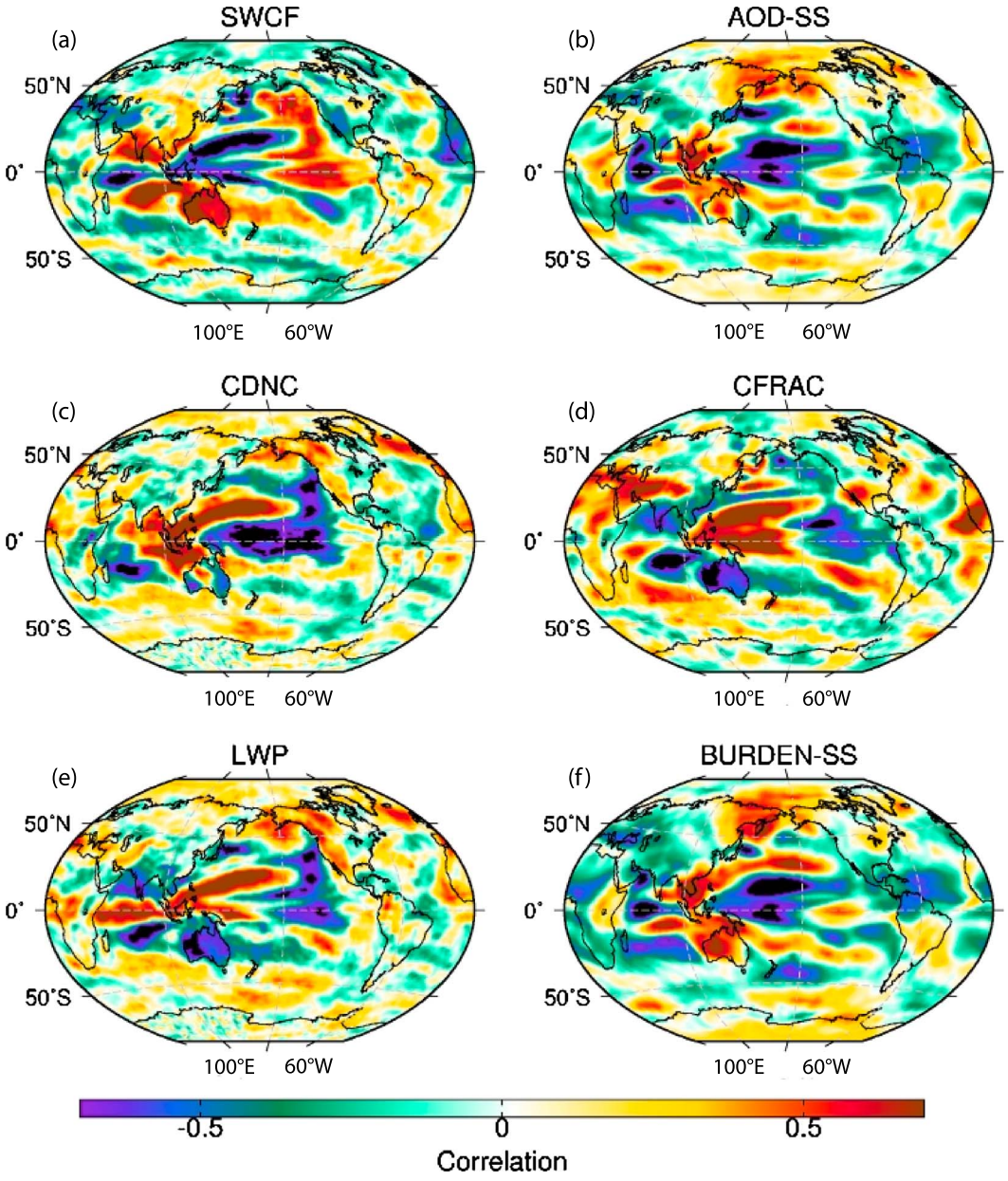

Figure 12. The calculated correlation coefficient between (a) shortwave cloud radiative forcing, (b) sea salt aerosol optical depth, (c) column-integrated cloud droplet number, (d) total cloud fraction, (e) cloud liquid water path, and (f) sea salt burden and the modeled PDO index for the cold season (i.e., October-November-December-January-February-March).

3.3. Decadal Variability of Sea Salt Aerosols

Besides the interannual variability, decadal climate variability can have an important impact on ecosystems and society. In fact, numerical experiments to support the most recent IPCC report include a set of decadal prediction experiments [*Taylor et al.,* 2012]. Recognizing this importance, we examine here the decadal variability of sea salt and their related cloud and radiative properties.

Figure 10 shows the time series of the principal components associated with EOF 1 obtained by applying a 10 year low-pass filter to the sea salt burden, 10 m wind speed, column-integrated cloud droplet number, and shortwave cloud radiative forcing prior to computing the EOFs. By employing a 10 year low-pass filter using a Lanczos response function [*Duchon*, 1979], the high-frequency variability larger than 0.1 cycles per year is attenuated. As expected, Figure 10 shows that the low-frequency evolution of these

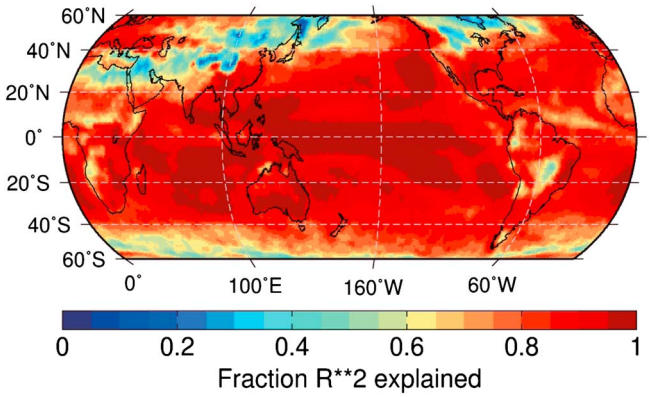

Figure 13. The coefficient of determination (i.e., R^2) of the regression fit given in equation (1). The global average value between 60°S and 60°N is 0.81.

quantities is consistent across the different variables, confirming that the close interaction among sea salt aerosol, clouds, and radiation seen above is unchanged on decadal timescales. A power spectrum of the filtered data shows no statistically significant spectral peak is present at decadal timescales (not shown).

On the multiyear to decadal timescales, the Pacific Decadal Oscillation (PDO) and Atlantic Multidecadal Oscillation (AMO) are well-known examples of internal natural variability. The AMO is associated with variations in Atlantic hurricanes, tropical rainfall, and North American and European summer climate [*Trenberth and Shea*, 2006; *Knight et al.*, 2006; *Zhang and Delworth*, 2006; *Sutton and Hodson*, 2007]. The AMO has also been linked to atmospheric aerosols [*Booth et al.*, 2012]. In this study, the PDO index that is based on the first EOF mode of sea surface temperature over the North Pacific (20°N to 70°N, 110°E to 260°E) is computed [*Mantua et al.*, 1997; *Zhang et al.*, 1997]. The PDO is more or less the North Pacific manifestation of the IPO [*Folland et al.,* 2002] and has been shown to be associated with variations in North American climate [e.g., *Gershunov and Barnett,* 1998; *Biondi et al.,* 2001]. Following the approach given in *Trenberth and Shea* [2006], the modeled AMO index is derived by smoothing a 10 year running mean of sea surface temperature anomalies averaged over the North Atlantic (0 to 60°N, 0 to 80°W) for the simulated 150 years. Figures 11 and 12 show the correlation coefficient between anomalies in shortwave cloud radiative forcing, sea salt aerosol optical depth, column-integrated cloud droplet number, total cloud fraction, cloud liquid water path, sea salt burden, and the AMO and PDO indices, respectively. To be consistent, the variables are low-pass filtered in the same way used when constructing the AMO and PDO indices, so the limitation of only having ~15 independent samples must be kept in mind. The sea salt optical depth, burden, and shortwave cloud forcing anomalies are strongly correlated with the AMO index over the Northern Atlantic Ocean with the coefficient value ~0.6, while the other three variables (cloud droplet number, cloud fraction, and liquid water path) show negative correlation in the same region. In the Pacific Ocean (Figure 12), the sea salt optical depth, burden, and shortwave cloud forcing display strong positive correlation with the PDO index over the eastern Pacific and negative correlation over the western Pacific, while the correlation between three cloud-related variables and the PDO index show an opposite sign. Overall, these patterns indicate that the modeled sea salt aerosol and cloud and radiation-related properties in CESM have signatures on multiyear to decadal timescales that are consistent with the model's PDO and AMO.

Change in shortwave cloud radiative forcing have strong effects on climate and may result from changes in aerosols along with consequent changes in cloud droplet number, cloud fraction, and liquid water path. We use a multivariate regression to estimate the contribution of variations in our explanatory variables (sea salt aerosol optical depth, cloud droplet number, cloud fraction, and cloud liquid water path) to variations in shortwave radiative forcing. A general model relating these quantities can be written in the form

$$\ln(\mathrm{SWCF}(t)) = \beta_0 + \beta_1 \ln(\mathrm{AODSS}(t)) + \beta_2 \ln(\mathrm{CDNC}(t)) + \beta_3 \ln(\mathrm{CF}(t)) + \beta_4 \ln(\mathrm{LWP}(t)) + \varepsilon \quad (1)$$

where SWCF(t), AODSS(t), CDNC(t), CF(t), and LWP(t) are the monthly anomalies of shortwave cloud radiative forcing, sea salt aerosol optical depth, column-integrated cloud droplet number concentration, cloud fraction, and liquid water path at a given location and ε is an error term. The formulation in terms of the logs of quantities is chosen based on our a priori assumption that variations in shortwave cloud forcing are affected by the product of the explanatory variables; however, as a sensitivity test we also tried a simple linear formulation and found that the results changed a little. The regression coefficients β_0, β_1, …, β_4 are determined by a least squares fit. The total variance explained by the regression (R^2) at each point is shown in Figure 13; the regression accounts for approximately 81% of shortwave cloud forcing variance averaged over regions between 60°S and 60°N.

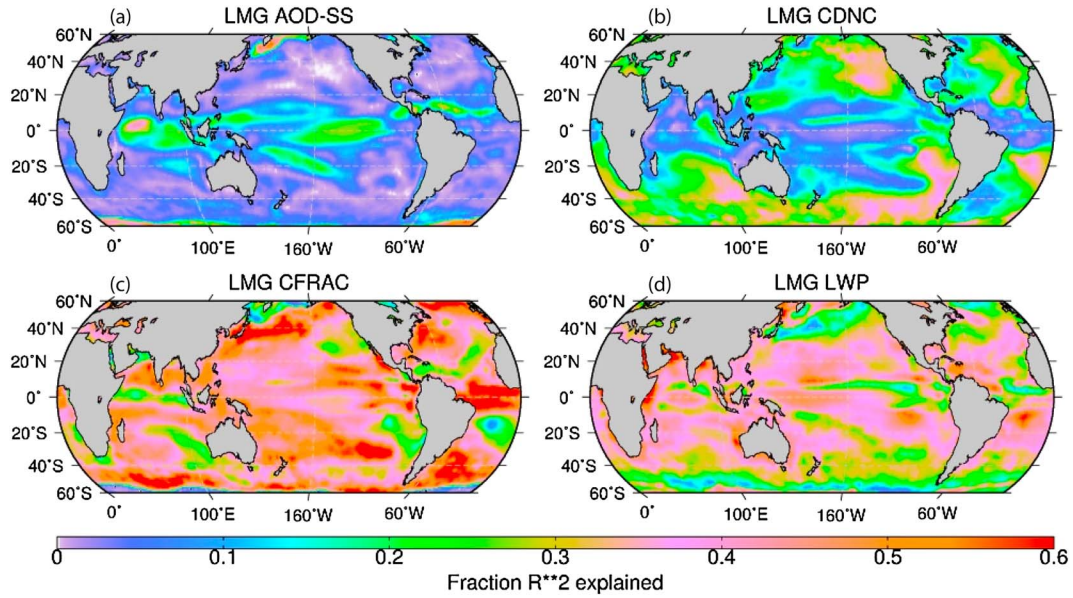

Figure 14. The LMG method for estimated fraction of annual variance in shortwave cloud forcing explained by (a) sea salt aerosol optical depth (AODSS), (b) column-integrated cloud droplet number concentration (CDNC), (c) cloud fraction, and (d) cloud liquid water path. Values are not calculated over the polar regions because some of the required data were not retained in the winter polar regions.

The explanatory variables can have appreciable covariability; for example, the correlation between sea salt aerosol optical depth and cloud droplet number concentration anomalies exceeds 0.7 in the western Pacific and eastern Indian Oceans. To better understand how the explanatory variables contribute to SWCF variability given these relationships, we use the LMG (Lindeman, Merenda and Gold) method [*Grömping*, 2006; *Lindeman et al.,* 1980]. The LMG approach is particularly appropriate when the explanatory variables have nontrivial correlations between them and physical processes link the explanatory variables [*Grömping*, 2006], as is the case here.

Figure 14a shows that variability in sea salt aerosols accounts for about 20–30% of the variability in shortwave cloud forcing over the tropical oceans, while roughly 20–30% variance of shortwave cloud forcing over Northern and Southern Ocean is associated with cloud droplet number concentration (Figure 14b). Cloud fraction and liquid water path play more significant global roles, accounting for 35–45% of the total global shortwave cloud radiative forcing variance (Figures 14c and 14d).

4. Conclusions

Previous work has identified the importance of quantifying the variability of natural aerosols, given their role in affecting climate through direct (reflection and absorption) and indirect (cloud-mediated) effects. Although such climate variability proceeds on many timescales, interannual to decadal timescales can be of particular importance to society through the effects on agriculture, drought, and ecosystems. The objective of this study is to investigate the leading global patterns of interannual to decadal variability of sea salt aerosols in a preindustrial environment. Since the multidecadal records needed to explore this question are not available from observations, we have employed a 150 year simulation for the preindustrial conditions using the Community Earth System Model version 1.0 (CESM1). We have additionally examined how sea salt aerosol variability contributes to the variability of shortwave cloud forcing (SWCF), since sea salt aerosol constitutes one of the largest aerosol mass burdens among all natural aerosols.

The results show that at interannual timescales, global patterns of sea salt, and related cloud and radiative properties are primarily responding to the ENSO cycle, with the largest spatial patterns of coherent variability found primarily in the tropical Pacific. This is true even though the greatest sea salt atmospheric burdens are found in the Southern Ocean. The relationship between ENSO and the total burden of sea

saltaerosols arises primarily through the modulation of surface emissions of sea salt via ENSO's effects on wind speed. ENSO-related ocean surface temperature changes also affect sea salt emissions, but the effect due to ENSO-related wind changes is relatively larger. The effect of changes in the deposition rate on total burden, which are associated with change in precipitation along the equator in the Pacific and eastern Indian Oceans with the ENSO cycle, are of lesser importance but can also be seen. Although we have found a significant influence of sea salt on the ENSO signature of cloud radiative forcing, definitive conclusions about the role of the aerosol-cloud interactions in ENSO will require simulations without interannual variability in sea salt emission.

At decadal timescales, the model exhibits variability similar to the observed Pacific Decadal Oscillation (PDO) and Atlantic Multidecadal Oscillation (AMO), as has been noted by previous studies [*Allen et al.*, 2014; *Booth et al.*, 2012]. Variations in sea salt aerosol and cloud properties are correlated with the PDO and AMO indices at levels of ~0.6, although there is no statistically significant spectral peak in variance at the decadal timescales, unlike at the ENSO frequencies. The modeled atmospheric variables' correlation patterns with SST variability tend to be symmetric about the equator and have significant expression in the extratropics, similar to the Interdecadal Pacific Oscillation (IPO). An IPO-like pattern is also seen in the relationship between observed sea salt aerosol and SST anomalies, although there are only five sea salt aerosol measurement stations available in the Pacific basin for the analysis and the period of observation is only ~20 years.

The statistical analysis used here suggests that sea salt aerosols may account for 20–30% of the variability in shortwave cloud forcing in the tropical Pacific on interannual timescales. Outside of the tropics, sea salt aerosol variability has negligible contribution to the interannual variability of SWCF. This is mainly ascribed to the fact that sea salt particles, in general, are not a major contributor to the CCN number population except under particular circumstances, for instance, in the remote ocean at specific times where wind speeds are high and/or other aerosol sources are low [*Andreae and Rosenfeld*, 2008]. As noted in *Lewis and Schwartz* [2004], the global average sea salt aerosol number concentration (1–30 cm^{-3}) is much smaller than the typical remote marine aerosol number concentrations in the CCN size range (70–220 cm^{-3}) [*Heintzenberg et al.*, 2000]. In addition, cloud albedo responds to the fractional change of cloud droplet number concentrations instead of their absolute change [*Rap et al.*, 2013]. As reported in *Rap et al.* [2013], sea salt aerosol contributes the smallest impact on clouds ($-0.04\ W\ m^{-2}$) among all other natural aerosols (e.g., DMS-originated sulfate, volcanic sulfate, terpene secondary organic aerosol, and wildfire) despite the largest atmospheric burden owing to its least contribution to cloud droplet number concentration (~1.3%) and its smallest indirect effect burden efficiency (i.e., the radiative effect at the top of atmosphere per unit aerosol burden). This explains why small variations of sea salt burden (e.g., outside of the tropics shown in Figure 1b) generally do not significantly impact clouds and radiation.

Different models have shown different sensitivity of sea salt aerosols to climate changes. *Mahowald et al.* [2006] used the Community Atmospheric Model version 3 to show that global averaged emissions, burden, and deposition of modeled sea salt aerosols are not very sensitive (<5%) to changes that occurred in past, present, and future climates, while another model simulation by *Korhonen et al.* [2010] suggested that the sensitivity of sea salt aerosols to the variation in wind fields was larger, as was also indicated in ice core records [*Wolff et al.*, 2006].

Since sea salt aerosols represent a significant source of natural aerosols and natural aerosols represent background aerosol concentrations [*Andreae and Rosenfeld*, 2008], more studies are required to investigate the variation of sea salt aerosols with changing climates as well as potential climate feedbacks on natural aerosols (such as sea salt) in terms of interannual or decadal timescales. In particular, our results obtained from a regression between sea salt aerosols and shortwave cloud forcing show that targeted, mechanistic model experiments examining the causal influence of interannual sea salt variability on shortwave cloud forcing in the tropical Pacific would be worthwhile. Such detailed, process-oriented studies are a prerequisite for us to sufficiently understand the impacts of aerosols with anthropogenic origins on clouds and climate in the future.

Acknowledgments

This research was supported by NSF AGS1048995 and by DOE DE-SC0006679 as part of the U.S. Department of Energy, Office of Science, Biological and Environmental Research, Decadal and Regional Climate Prediction using Earth System Models (EaSM) program. The Pacific Northwest National Laboratory is operated for the DOE by Battelle Memorial Institute under contract DE-AC05-76RLO 1830. We are grateful for the NASA MEaSUREs project providing the SeaWiFS AOD satellite data and for Joseph M. Prospero and Michael Schulz providing the long-term measurements of aerosols over the global ocean. All model results are available at http://portal.nersc.gov/project/m1374/SeaSalt/ in the National Energy Research Scientific Computing Center (NERSC).

References

Albrecht, B. A. (1989), Aerosols, cloud microphysics, and fractional cloudiness, *Science*, *245*, 1227–1230.

Allen, R. J., J. R. Norris, and M. Kovilakam (2014), Influence of anthropogenic aerosols and the Pacific Decadal Oscillation on tropical belt width, *Nat. Geosci.*, *7*, 270–274, doi:10.1038/ngeo2091.

Andreae, M. O., and D. Rosenfeld (2008), Aerosol–cloud–precipitation interactions. Part 1: The nature and sources of cloud-active aerosols, *Earth Sci. Rev.*, *89*, 13–41.
Biondi, F., A. Gershunov, and D. R. Cayan (2001), North Pacific decadal climate variability since 1661, *J. Clim.*, *14*, 5–10.
Booth, B. B. B., N. J. Dunstone, P. R. Halloran, T. Andrews, and N. Bellouin (2012), Aerosols implicated as a prime driver of twentieth-century North Atlantic climate variability, *Nature*, *484*, 228–232.
Boucher, O., et al. (2013), Clouds and Aerosols, in *Climate Change 2013: The Physical Science Basis. Contribution of Working Group I to the Fifth Assessment Report of the Intergovernmental Panel on Climate Change*, edited by T. F. Stocker et al., Cambridge Univ. Press, Cambridge, U. K., and New York.
Carslaw, K. S., et al. (2013), Large contribution of natural aerosols to uncertainty in indirect forcing, *Nature*, *503*, 67–71, doi:10.1038/nature12674.
Chandra, S., J. R. Ziemke, J. R. Min, and W. G. Read (1998), Effects of 1997–1998 El Niño on tropospheric ozone and water vapor, *Geophys. Res. Lett.*, *25*, 3867–3870, doi:10.1029/98GL02695.
Chandra, S., J. R. Ziemke, B. N. Duncan, T. L. Diehl, N. J. Livesey, and L. Froidevaux (2009), Effects of the 2006 El Niño on tropospheric ozone and carbon monoxide: Implications for dynamics and biomass burning, *Atmos. Chem. Phys.*, *9*, 4239–4249, doi:10.5194/acp-9-4239-2009.
Clarke, A. D., S. R. Owens, and J. Zhou (2006), An ultrafine sea-salt flux from breaking waves: Implications for cloud condensation nuclei in the remote marine atmosphere, *J. Geophys. Res.*, *111*, D06202, doi:10.1029/2005JD006565.
Deser, C., A. S. Phillips, R. A. Tomas, Y. M. Okumura, M. A. Alexander, A. Capotondi, J. D. Scott, Y.-O. Kwon, and M. Obha (2012), ENSO and Pacific decadal variability in Community Climate System Model Version 4, *J. Clim.*, *25*, 2622–2651.
Duchon, C. E. (1979), Lanczos filtering in one and two dimensions, *J. Appl. Meteor.*, *18*, 1016–1022, doi:10.1175/1520-0450(1979)018<1016:LFIOAT>2.0.CO;2.
Flato, G., et al. (2013), Evaluation of climate models, in *Climate Change 2013: The Physical Science Basis. Contribution of Working Group I to the Fifth Assessment Report of the Intergovernmental Panel on Climate Change*, edited by T. F. Stocker et al., Cambridge Univ. Press, Cambridge, U. K., and New York.
Folland, C. K., J. A. Renwick, M. J. Salinger, and A. B. Mullan (2002), Relative influences of the Interdecadal Pacific Oscillation and ENSO on the South Pacific convergence zone, *Geophys. Res. Lett.*, *29*(13), 1643, doi:10.1029/2001GL014201.
Gershunov, A., and T. P. Barnett (1998), Interdecadal modulation of ENSO teleconnections, *Bull. Am. Meteorol. Soc.*, *79*, 2715–2725.
Ghan, S. J., S. J. Smith, M. Wang, K. Zhang, K. Pringle, K. Carslaw, J. Pierce, S. Bauer, and P. Adams (2013), A simple model of global aerosol indirect effects, *J. Geophys. Res. Atmos.*, *118*, 1–20, doi:10.1002/jgrd.50567.
Grömping, U. (2006), Relative importance for linear regression in R: The package relaimpo, *J. Stat.*, *17*(1).
Grythe, H., J. Ström, R. Krejci, P. Quinn, and A. Stohl (2013), A review of sea spray aerosol source functions using a large global set of sea salt aerosol concentration measurements, *Atmos. Chem. Phys. Discuss.*, *13*, 20,729–20,781, doi:10.5194/acpd-13-20729-2013.
Heintzenberg, J., D. C. Covert, and R. Van Dingenen (2000), Size distribution and chemical composition of marine aerosols: A compilation and review, *Tellus, Ser. B*, *52*, 1104–1122.
Hsu, N. C., R. Gautam, A. M. Sayer, C. Bettenhausen, C. Li, M. J. Jeong, S.-C. Tsay, and B. N. Holben (2012), Global and regional trends of aerosol optical depth over land and ocean using SeaWiFS measurements from 1997 to 2010, *Atmos. Chem. Phys.*, *12*, 8037–8053, doi:10.5194/acp-12-8037-2012.
Hurrell, J. W., et al. (2013), The Community Earth System Model: A framework for collaborative research, *Bull. Am. Meteorol. Soc.*, *94*, 1339–1360, doi:10.1175/BAMS-D-12-00121.
Jones, A., J. M. Haywood, and O. Boucher (2007), Aerosol forcing, climate response and climate sensitivity in the Hadley Centre climate model, *J. Geophys. Res.*, *112*, D20211, doi:10.1029/2007JD008688.
Knight, J. R., C. K. Folland, and A. A. Scaife (2006), Climate impacts of the Atlantic Multidecadal Oscillation, *Geophys. Res. Lett.*, *33*, L17706, doi:10.1029/2006GL026242.
Korhonen, H., K. S. Carslaw, and S. Romakkaniemi (2010), Enhancement of marine cloud albedo via controlled sea spray injections: A global model study of the influence of emission rates, microphysics and transport, *Atmos. Chem. Phys.*, *10*, 4133–4143, doi:10.5194/acp-10-4133-2010.
Latham, J., and M. H. Smith (1990), Effect on global warming of wind dependent aerosol generation at the ocean surface, *Nature*, *347*, 372–373, doi:10.1038/347372a0.
Le Page, Y., J. M. C. Pereira, R. Trigo, C. da Camara, D. Oom, and B. Mota (2008), Global fire activity patterns (1996–2006) and climatic influence: An analysis using the World Fire Atlas, *Atmos. Chem. Phys.*, *8*, 1911–1924, doi:10.5194/acp-8-1911-2008.
Lewis, E. R., and S. E. Schwartz (2004), *Sea Salt Aerosol Production: Mechanisms, Methods, Measurements, and Models—A Critical Review*, AGU, Washington, D. C.
Li, J., B. E. Carlson, and A. A. Lacis (2011), El Niño–Southern Oscillation correlated aerosol Ångström exponent anomaly over the tropical Pacific discovered in satellite measurements, *J. Geophys. Res.*, *116*, D20204, doi:10.1029/2011JD015733.
Lindeman, R. H., P. F. Merenda, and R. Z. Gold (1980), *Introduction to Bivariate and Multivariate Analysis*, Scott, Foresman, Glenview, Ill.
Liu, X., et al. (2012), Toward a minimal representation of aerosols in climate models: Description and evaluation in the Community Atmosphere Model CAM5, *Geosci. Model Dev.*, *5*, 709–739, doi:10.5194/gmd-5-709-2012.
Logan, J. A., I. Megretskaia, R. Nassar, L. T. Murray, L. Zhang, K. W. Bowman, H. M. Worden, and M. Luo (2008), Effects of the 2006 El Niño on tropospheric composition as revealed by data from the Tropospheric Emission Spectrometer (TES), *Geophys. Res. Lett.*, *35*, L03816, doi:10.1029/2007GL031698.
Mahowald, N. M., J.-F. Lamarque, X. X. Tie, and E. Wolff (2006), Sea salt aerosol response to climate change: Last Glacial Maximum, preindustrial, and doubled carbon dioxide climates, *J. Geophys. Res.*, *111*, D05303, doi:10.1029/2005JD006459.
Mantua, N. J., S. R. Hare, Y. Zhang, J. M. Wallace, and R. C. Francis (1997), A Pacific interdecadal climate oscillation with impacts on salmon production, *Bull. Am. Meteorol. Soc.*, *78*, 1069–1079.
Marlier, M. E., R. S. DeFries, A. Voulgarakis, P. L. Kinney, J. T. Randerson, D. T. Shindell, Y. Chen, and G. Faluvegi (2013), El Niño and health risks from landscape fire emissions in southeast Asia, *Nat. Clim. Change*, *3*, 131–136, doi:10.1038/nclimate1658.
Martensson, E. M., E. D. Nilsson, G. de Leeuw, L. H. Cohen, and H.-C. Hansson (2003), Laboratory simulations and parameterization of the primary marine aerosol production, *J. Geophys. Res.*, *108*(D9), 4297, doi:10.1029/2002JD002263.
Mitchell, R. M., S. K. Campbell, and Y. Qin (2010), Recent increase in aerosol loading over the Australian arid zone, *Atmos. Chem. Phys.*, *10*, 1689–1699, doi:10.5194/acp-10-1689-2010.
Monahan, E., D. Spiel, and K. Davidson (1986), A model of marine aerosol generation via whitecaps and wave disruption, in *Oceanic Whitecaps and Their Role in Air–Sea Exchange*, pp. 167–174, D. Reidel, Norwell, Mass.
Morrison, H., and A. Gettelman (2008), A new two-moment bulk stratiform cloud microphysics scheme in the community atmosphere model, version 3 (CAM3). Part I: Description and numerical tests, *J. Clim.*, *21*, 3642–3659.
O'Dowd, C., M. H. Smith, I. E. Consterdine, and J. A. Lowe (1997), Marine aerosol, sea salt, and the marine sulphur cycle: A short review, *Atmos. Environ.*, *31*, 73–80.

Park, S., and C. S. Bretherton (2009), The University of Washington shallow convection and moist turbulence schemes and their impact on climate simulations with the community atmosphere model, *J. Clim.*, *22*, 3449–3469.
Park, S., C. S. Bretherton, and P. J. Rasch (2014), Integrating cloud processes in the Community Atmosphere Model, version 5, *J. Clim.*, *27*, 6821–6856, doi:10.1175/JCLI-D-14-00087.1.
Parker, D., C. Folland, A. Scaife, J. Knight, A. Colman, P. Baines, and B. Dong (2007), Decadal to multidecadal variability and the climate change background, *J. Geophys. Res.*, *112*, D18115, doi:10.1029/2007JD008411.
Penner, J. E., et al. (2001), Aerosols, their direct and indirect effects, in *Climate Change 2001: The Scientific Basis, Contribution of Working Group I to the Third Assessment Report of the Intergovernmental Panel on Climate Change*, edited by J. T. Houghton et al., chap. 5, pp. 289–348, Cambridge Univ. Press, Cambridge, U. K.
Penner, J. E., L. Xu, and M. Wang (2011), Satellite methods underestimate indirect climate forcing by aerosols, *Proc. Natl. Acad. Sci. U.S.A.*, *108*, 13,404–13,408.
Penner, J. E., C. Zhou and L. Xu (2012), Consistent estimates from satellites and models for the first aerosol indirect forcing, *Geophys. Res. Lett.*, *39*, L13810, doi:10.1029/2012GL051870.
Power, S., T. Casey, C. Folland, A. Colman, and V. Mehta (1999), Inter-decadal modulation of the impact of ENSO on Australia, *Clim. Dyn.*, *15*, 319–324.
Prospero, J. M., and P. J. Lamb (2003), African droughts and dust transport to the Caribbean: Climate change implications, *Science*, *302*, 1024–1027, doi:10.1126/science.1089915.
Rap, A., C. E. Scott, D. V. Spracklen, N. Bellouin, P. M. Forster, K. S. Carslaw, A. Schmidt, and G. Mann (2013), Natural aerosol direct and indirect radiative effects, *Geophys. Res. Lett.*, *40*, 3297–3301, doi:10.1002/grl.50441.
Shen, S. S. P., N. Tafolla, T. M. Smith, and P. A. Arkin (2014), An estimate of sampling errors in the reconstruction of global annual precipitation from 1900–2011, *J. Atmos. Sci.*, doi:10.1175/JAS-D-13-0301.1.
Spada, M., O. Jorba, C. Pérez García-Pando, Z. Janjic, and J. M. Baldasano (2013), Modeling and evaluation of the global sea-salt aerosol distribution: Sensitivity to size-resolved and sea-surface temperature dependent emission schemes, *Atmos. Chem. Phys.*, *13*, 11,735–11,755, doi:10.5194/acp-13-11735-2013.
Struthers, H., A. M. L. Ekman, P. Glantz, T. Iversen, A. Kirkevåg, Ø. Seland, E. M. Mårtensson, K. Noone, and E. D. Nilsson (2013), Climate-induced changes in sea salt aerosol number emissions: 1870 to 2100, *J. Geophys. Res. Atmos.*, *118*, 670–682, doi:10.1002/jgrd.50129.
Sutton, R. T., and D. L. R. Hodson (2007), Climate response to basin-scale warming and cooling of the North Atlantic Ocean, *J. Clim.*, *20*, 891–907, doi:10.1175/JCLI4038.1.
Taylor, K. E., R. J. Stouffer, and G. A. Meehl (2012), An overview of CMIP5 and the experiment design, *Bull. Am. Meteorol. Soc.*, *93*, 485–498.
Textor, C., et al. (2006), Analysis and quantification of the diversities of aerosol life cycles within AeroCom, *Atmos. Chem. Phys.*, *6*, 1777–1813, doi:10.5194/acp-6-1777-2006.
Trenberth, K. E., and D. J. Shea (2006), Atlantic hurricanes and natural variability in 2005, *Geophys. Res. Lett.*, *33*, L12704, doi:10.1029/2006GL026894.
Twomey, S. (1974), Pollution and the planetary albedo, *Atmos. Environ.*, *8*, 1251–1256.
van der Werf, G. R., J. T. Randerson, L. Giglio, J. G. Collatz, P. Kasibhatla, and A. F. Arellano (2006), Interannual variability in global biomass burning emissions from 1997 to 2004, *Atmos. Chem. Phys.*, *6*, 3423–3441, doi:10.5194/acp-6-3423-2006.
Wilcox, L., E. Highwood, and N. Dunstone (2013), The influence of anthropogenic aerosol on multi-decadal variations of historical global climate, *Environ. Res. Lett.*, *8*, doi:10.1088/1748-9326/8/2/024033.
Wolff, E., et al. (2006), Southern Ocean sea-ice extent, productivity and iron flux over the past eight glacial cycles, *Nature*, *440*, 491–496.
Wu, R., Z. Wen, and Z. He (2013), ENSO contribution to aerosol variations over the maritime continent and the Western North Pacific during 2000–10, *J. Clim.*, *26*, 6541–6560.
Young, I. R., S. Zieger, and A. V. Babanin (2011), Global trends in wind speed and wave height, *Science*, *332*, 451–455.
Zhang, G. J., and N. A. McFarlane (1995), Sensitivity of climate simulations to the parameterization of cumulus convection in the Canadian Climate Center general circulation model, *Atmos. Ocean*, *33*, 407–446.
Zhang, R., and T. L. Delworth (2006), Impact of Atlantic Multidecadal oscillations on India/Sahel rainfall and Atlantic hurricanes, *Geophys. Res. Lett.*, *33*, L17712, doi:10.1029/2006GL026267.
Zhang, R., et al. (2013), Have aerosols caused the observed Atlantic multidecadal variability?, *J. Atmos. Sci.*, *70*, 1135–1144, doi:10.1175/JAS-D-12-0331.1.
Zhang, Y., J. M. Wallace, and D. S. Battisti (1997), ENSO-like interdecadal variability: 1900–93, *J. Clim.*, *10*, 1004–1020.